The Astrophysical Journal Letters, 746:L2 (6pp), 2012 February 10 doi:10.1088/2041-8205/746/1/L2

ON THE NATURE OF THE HERBIG B[e] STAR BINARY SYSTEM V921 SCORPII: DISCOVERY OF A CLOSE COMPANION AND RELATION TO THE LARGE-SCALE BIPOLAR NEBULA*

Stefan Kraus[1], Nuria Calvet[1], Lee Hartmann[1], Karl-Heinz Hofmann[2], Alexander Kreplin[2], John D. Monnier[1], and Gerd Weigelt[2]
[1] Department of Astronomy, University of Michigan, 918 Dennison Building, Ann Arbor, MI 48109-1090, USA
[2] Max Planck Institut für Radioastronomie, Auf dem Hügel 69, 53121 Bonn, Germany
Received 2011 December 13; accepted 2012 January 3; published 2012 January 18

ABSTRACT

Belonging to the group of B[e] stars, V921 Scorpii is associated with a strong infrared excess and permitted and forbidden line emission, indicating the presence of low- and high-density circumstellar gas and dust. Many aspects of V921 Sco and other B[e] stars still remain mysterious, including their evolutionary state and the physical conditions resulting in the class-defining characteristics. In this Letter, we employ Very Large Telescope Interferometer/AMBER spectro-interferometry in order to reconstruct high-resolution ($\lambda/2B = 0\farcs0013$) model-independent interferometric images for three wavelength bands around 1.65, 2.0, and 2.3 μm. In our images, we discover a close (25.0 ± 0.8 mas, corresponding to $\sim 29 \pm 0.9$ AU at 1.15 kpc) companion around V921 Sco. Between two epochs in 2008 and 2009, we measure orbital motion of $\sim 7^\circ$, implying an orbital period of $\sim$35 years (for a circular orbit). Around the primary star, we detect a disk-like structure with indications for a radial temperature gradient. The polar axis of this AU-scale disk is aligned with the arcminute-scale bipolar nebula in which V921 Sco is embedded. Using Magellan/IMACS imaging, we detect multi-layered arc-shaped substructure in the nebula, suggesting episodic outflow activity from the system with a period of $\sim$25 years, roughly matching the estimated orbital period of the companion. Our study supports the hypothesis that the B[e] phenomenon is related to dynamical interaction in a close binary system.

Key words: accretion, accretion disks – binaries: close – protoplanetary disks – stars: individual (V921 Scorpii) – stars: pre-main sequence – techniques: interferometric

Online-only material: color figures

1. INTRODUCTION

B[e] stars are intermediate-mass stars associated with substantial amounts of circumstellar gas and dust, as indicated by permitted and forbidden line emission, in particular of [O I] and [Fe II], and a strong infrared excess (Allen & Swings 1976). These class-defining characteristics have been observed in a wide range of evolutionary stages (Lamers et al. 1998), including pre-main-sequence stars (Herbig Ae/B[e]), post-main-sequence stars (supergiants, symbiotic stars, or compact planetary nebulae), and stars of unknown nature (unclassified B[e] stars). In the pre-main-sequence stage, about half of all intermediate-mass young stars show the *B[e] phenomenon* (Oudmaijer et al. 2006), although significant differences in the strength of the forbidden line emission can be observed.

It has been proposed that the B[e] phenomenon might be related to the presence of a close binary system, where the line-emitting gas is ejected in recurring mass-loss events triggered by the companion (e.g., Sheikina et al. 2000; Miroshnichenko 2007). To test this hypothesis, it is important to search for close companions around B[e] stars. Given the kiloparsec distance of B[e] stars, this task requires high angular resolution, which we achieve in this Letter using infrared interferometry.

We observed the unclassified B[e] star V921 Sco using the Very Large Telescope Interferometer (VLTI). The AU-scale environment around this B0Ve-type star has been investigated by two earlier interferometric studies, which determined the spatial extension of the Brγ-line-emitting region (Kraus et al. 2008) and the structure of the continuum-emitting disk (Kreplin et al. 2012). V921 Sco is associated with an intriguing nebula, which shows reflection as well as absorption characteristics (Hutsemekers & van Drom 1990) and which has been imaged both at visual (Hutsemekers & van Drom 1990) and mid-infrared wavelengths (Boersma et al. 2009). There is some debate on the distance ($\sim$1.15 kpc; Borges Fernandes et al. 2007) and nature of V921 Sco, with authors arguing both for an evolved (Hutsemekers & van Drom 1990; Borges Fernandes et al. 2007) and young (Benedettini et al. 1998; Habart et al. 2003; Acke et al. 2005; Acke & van den Ancker 2006) evolutionary stage.

In this Letter, we report on Magellan wide-field imaging and VLTI aperture synthesis imaging observations (Section 2), which reveal the presence of a close companion around V921 Sco. The astrometry of the binary system and the orientation of the circumprimary disk will be derived using quantitative modeling (Section 3) and interpreted in Section 4. A summary of our results is presented in Section 5.

2. OBSERVATIONS

2.1. VLTI/AMBER Spectro-interferometry

Our observations on V921 Sco were carried out using the AMBER instrument (Petrov et al. 2007), which allowed us to coherently combine the light from three of the VLTI 1.8 m auxiliary telescopes. The observations were conducted using AMBER's low spectral resolution mode, which covers the near-infrared H and K bands (1.44–2.50 μm) with a spectral resolution $R \sim 35$. The observations were carried out between 2008 April 3 and 2009 March 19 on four different array configurations (Table 1), providing a good uv-coverage with

* Based on observations made with ESO telescopes at the Paranal Observatory under the open-time programme ID 081.C-0706(A-D) and with the Magellan Baade and Clay telescopes.

Table 1
Observation Log of Our VLTI/AMBER Observations

Date (UT)	Time (UT)	NEXP	Telescope Triplet	Calibrator
2008 May 21	09:20	10	A0-D0-H0	HD 159941
2008 May 22	04:18	9	A0-D0-H0	HD 159941
2008 May 22	05:25	9	A0-D0-H0	HD 159941
2008 May 22	06:47	9	A0-D0-H0	HD 159941
2008 May 24	06:29	11	A0-D0-H0	HD 159941
2008 May 24	09:24	9	A0-D0-H0	HD 159941
2008 Sep 21	01:54	5	A0-K0-G1	HD 159941
2008 Apr 28	08:32	5	D0-H0-G1	HD 163197
2008 Apr 28	09:18	5	D0-H0-G1	HD 163197
2008 May 26	07:28	5	D0-H0-G1	HD 159941
2008 Jul 4	02:59	5	D0-H0-G1	HD 159941
2008 Jul 4	04:02	5	D0-H0-G1	HD 159941
2008 Jul 4	04:46	5	D0-H0-G1	HD 159941
2008 Jul 5	01:15	5	D0-H0-G1	HD 159941
2008 Jul 5	06:24	5	D0-H0-G1	HD 159941
2008 Apr 3	05:52	8	E0-G0-H0	HD 152040
2008 Apr 5	07:16	5	E0-G0-H0	HD 159941
2008 Apr 5	08:08	12	E0-G0-H0	HD 159941
2008 Jun 4	07:03	5	E0-G0-H0	HD 159941
2008 Jun 4	08:54	5	E0-G0-H0	HD 159941
2008 Jun 7	08:32	5	E0-G0-H0	HD 159941
2009 Feb 18	09:05	5	D0-H0-G1	HD 159941
2009 Feb 19	08:58	5	D0-H0-G1	HD 159941
2009 Mar 19	08:54	15	D0-H0-G1	HD 159941

Notes. NEXP lists the number of recorded exposures during each visit on the source, with each exposure consisting of 1000 individual interferograms. For the calibrators, we adopted the following uniform disk diameters: HD 106979: 0.886 ± 0.011 mas, HD 152040: 0.581 ± 0.04 mas (JMMC SearchCal); HD 145921: 0.957 ± 0.013 mas, HD 137730: 0.984 ± 0.014 mas (Mérand et al. 2006); HD 163197: 0.96 ± 0.01 mas, HD 159941: 1.09 ± 0.02 mas (Richichi et al. 2005).

baseline lengths between 10 and 127 m. For all observations, we used a detector integration time (DIT) of 100 ms.

For a significant fraction of our data we find that the closure phases (CPs) vary significantly between subsequent exposures (i.e., on timescales of several minutes). As discussed in Section 3, these rapid variations are very likely due to the presence of a companion star. Therefore, in contrast to the standard AMBER data reduction procedure, we decided not to average the individual exposures, but to fit the quantities derived from the individual data exposures separately.

Each observation on V921 Sco was accompanied by observations on interferometric calibrator stars of known intrinsic diameter, allowing us to monitor the instrumental and atmospheric transfer function. Both for the science and calibrator star observations, we extract raw visibilities and CPs using the amdlib (V3.0) data reduction software (Tatulli et al. 2007; Chelli et al. 2009). In order to associate the CP sign with the on-sky orientation, we use a reference data set[3] on the binary star θ^1 Orionis C (Kraus et al. 2009b).

2.2. Magellan/IMACS+FIRE Wide-field Imaging

In order to investigate the large-scale environment around V921 Sco, we employed the IMACS instrument on the Magellan/Baade 6.5 m telescope. The images were recorded on 2011 March 13 under exceptional atmospheric conditions (seeing FWHM $\sim$ 0.″4) and cover a field of 15.′4 with a pixel size of 0.″11 pixel^{-1}. We employed the Bessell B, V, and R filters and two narrowband filters centered around the [S II] and Hα line (filters "676circular" and "Halpha656") using DITs of 240 s, 240 s, 180 s, 300 s, and 360 s, respectively. The images were bias-subtracted and flat-fielded using standard IRAF data reduction routines and are shown in Figures 1(A)–(F).

Using the acquisition camera of the FIRE spectrograph (Simcoe et al. 2008) at Magellan/Clay we also recorded on 2011 March 12 a J-band image of V921 Sco (394 × 394 pixels with a pixel size 0.″147 pixel^{-1}), which is shown in Figure 1(H).

3. RESULTS

3.1. Aperture-synthesis Imaging

In order to derive the basic source structure of V921 Sco, we reconstructed model-independent aperture-synthesis images from our AMBER data. Since the object structure might change with wavelength, we subdivide our data set in three wavelength bins, which we denote with H ($1.4\,\mu\mathrm{m} \leqslant \lambda < 1.9\,\mu\mathrm{m}$), K_1 ($1.9\,\mu\mathrm{m} \leqslant \lambda < 2.15\,\mu\mathrm{m}$), and K_2 ($2.15\,\mu\mathrm{m} \leqslant \lambda < 2.5\,\mu\mathrm{m}$). For each wavelength bin, we reconstruct a separate image (Figure 2, top) and then combined the independent images in a color composite (Figure 2, bottom).

For the image reconstruction, we employed the building block mapping algorithm (Hofmann & Weigelt 1993), which was already used in several of our earlier long-baseline interferometric imaging projects (Kraus et al. 2007, 2009b, 2010b). The presented images were obtained without (Figure 2, left) and with (Figure 2, right) a regularization function. Image reconstruction with regularization means the minimization of the cost function

$$J[o_k(\mathbf{x})] := Q[o_k(\mathbf{x})] + \mu \cdot H[o_k(\mathbf{x})], \quad (1)$$

where $Q[o_k(\mathbf{x})]$ describes the χ^2 function of the measured bispectrum data $O^{(3)}(\mathbf{f_u}, \mathbf{f_v})$ and the bispectrum of the actual iterated image $o_k(\mathbf{x})$. $H[o_k(\mathbf{x})]$ is a regularization term, and μ is a weighting factor called the Lagrange multiplicator. For our reconstructions we used the maximum entropy regularization function

$$H[o_k(\mathbf{x})] := \int \left[o_k(\mathbf{x}) \cdot \log\left(\frac{o_k(\mathbf{x})}{p(\mathbf{x})}\right) - o_k(\mathbf{x}) + p(\mathbf{x}) \right] d\mathbf{x}. \quad (2)$$

As prior function $p(\mathbf{x})$ we used a smooth version of a building block reconstruction obtained without a regularization function ($\mu = 0$). The start image was a circumsymmetric Gaussian with a size obtained by fitting the measured visibilities. Reconstructions for different Lagrange multiplicators ($\mu = 10^{-6}$ to 10^{-3}) and for different reconstruction windows (radii: 60–100 mas) were obtained. The presented images are the best-fit reconstructions, i.e., those reconstructions with minimum reduced χ^2 values of the squared visibilities and CPs.

Each of the reconstructed images clearly reveals a close companion, which is located at a separation of $\sim$25 mas north of the primary star[4] ($\Theta \sim 353^\circ$) and which we denote in the following V921 Sco B. In our images, V921 Sco B appears point-like, while the primary star is clearly associated with extended emission that appears elongated along position angle (P.A.) $\phi \sim 145^\circ$. In the images, it is also evident that the contributions of V921 Sco B to the total flux decrease with wavelength.

[3] The reference data set can be accessed on the Web site http://www.skraus.eu/files/amber.htm.

[4] In this Letter, we define the primary star (=V921 Sco A) as the star associated with the majority of the near-infrared-emitting circumstellar material.

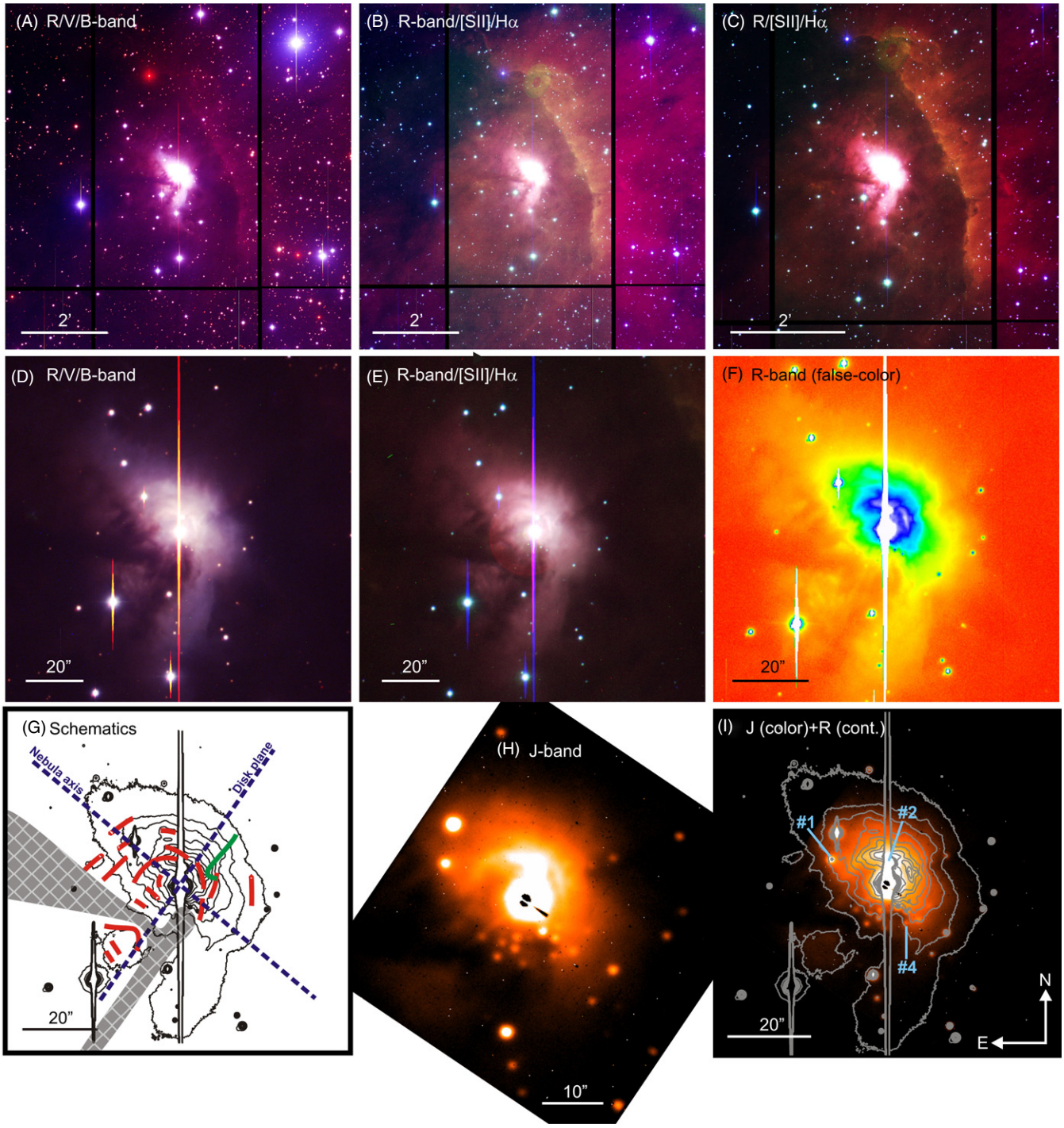

Figure 1. (A) and (D) Magellan/IMACS composite images of V921 Sco, taken in the filters Bessell-*R* (red), Bessell-*V* (green), and Bessell-*B* (blue) and shown for two different spatial scales. (B), (C), and (E) IMACS images for Bessell-*R* (red), [S II] (green), and Hα (blue). The black strips in panels (A) and (B) correspond to the gaps in the IMACS detector array. (F) IMACS image taken in Bessell-*R* filter, shown false colors in order to emphasize some arc-like substructures. (G) schematics, showing some of the filaments discovered in our IMACS images, overplotted on Bessell-*R* contours. (H) The *J*-band image recorded with the Magellan/FIRE acquisition camera and displayed with a heat color table and a square-root scaling. The FIRE spectrograph slit appears as a dark band roughly in the center of the image. (I) In the bottom right panel, we overplot the *J*-band image with the contours of the *R*-band image and also mark the location of the mid-infrared sources detected by Habart et al. (2003, source 3 was not clearly detected in our *J*-band image).

(A color version of this figure is available in the online journal.)

3.2. Model Fitting

In order to better characterize the geometry and physical conditions of the disk-like structure in our image and to derive the relative astrometry of V921 Sco A–B, we fitted geometric models to our interferometric data.

In all models, the primary star is included as a point source where the photospheric emission at a given wavelength is given by the flux ratio of a B0 ($T_{\rm eff}$ = 14,000 K, g = 4.04) Kurucz model atmosphere (Kurucz 1970) to the measured total SED flux $F_{\rm tot}$, with contributions $F_{\rm A}/F_{\rm tot}$ ranging from 0.27 (at 1.5 μm), 0.13 (at 2.0 μm) to 0.07 (at 2.5 μm), where $F_{\rm A}$ denotes the

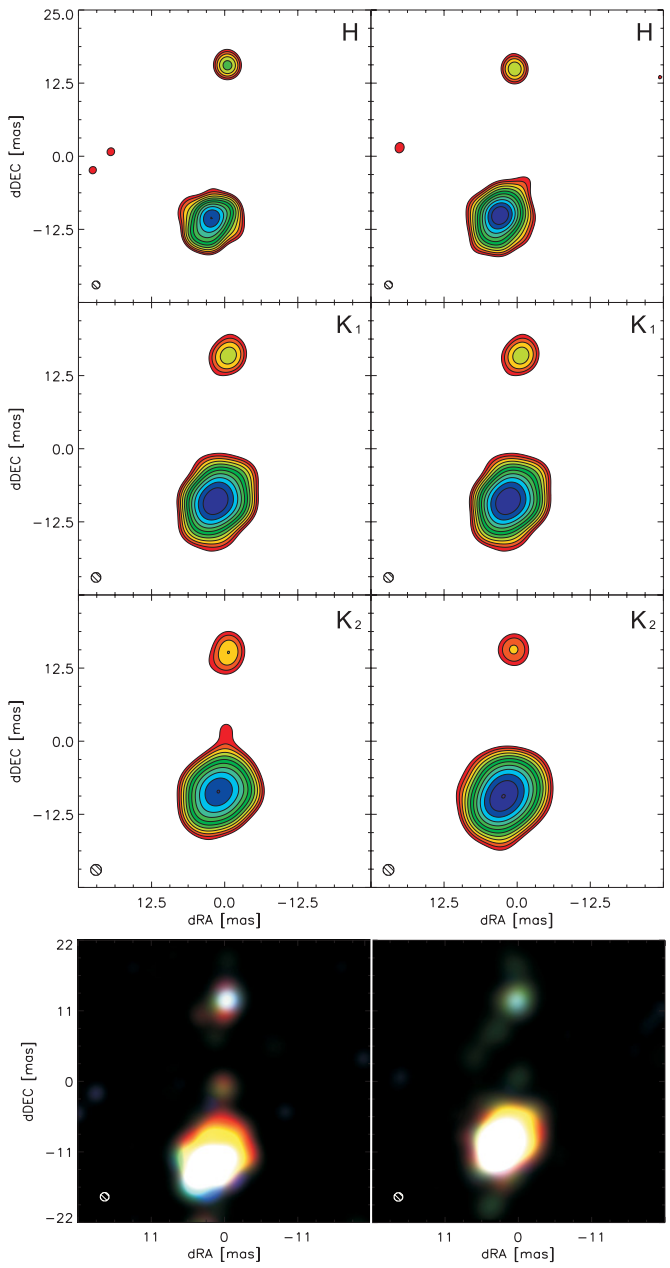

Figure 2. Aperture-synthesis images constructed without (left column) and with maximum entropy regularization (right column) from our VLTI/AMBER data for the H (top), K_1 (second from top), and K_2 (third from top) wavelength bins. The contours decrease from peak intensity by factors of $\sqrt{2}$. In the bottom row, the three wavelength bins are merged in a color composite (red: K_2, green: K_1, blue: H). All images were convolved to the formal resolution $\lambda/2B$, which is 1.3 mas (H), 1.6 mas (K_1), and 1.8 mas (K_2).

(A color version of this figure is available in the online journal.)

photospheric flux contribution of the primary star. We adopt $A_V = 4.8 \pm 0.2$, a stellar radius of $R_\star = 17.3 \pm 0.6\,R_\odot$, and a distance of $d = 1150 \pm 150$ pc (Borges Fernandes et al. 2007). Given that the spectral type of the primary was determined in earlier studies without knowledge of the companion star, we note that these spectral-type estimates are potentially biased, which could affect the photospheric flux of the primary star in our models. However, the absolute level and wavelength dependence of the photospheric emission in the near-infrared wavelength regime depend only weakly on the precise spectral type and will therefore not significantly affect our modeling results.

The companion star is described by five free parameters, namely, the P.A. (Θ) and separation (ρ) measured from the primary star, the angular extent of the circumstellar material (parameterized as Gaussians with FWHM θ_B), and two parameters ($(F_B/F_{tot})(\lambda_{ref})$, s) to describe the photospheric flux contributions of V921 Sco B to the total flux. The flux contributions might change with wavelength due to differences in the stellar effective temperatures, local extinction effects, or circumstellar emission. Given the still relatively short wavelength coverage, we approximate these effects with the linear relation $(F_B/F_{tot})(\lambda) = (F_B/F_{tot})(\lambda_{ref}) + s \cdot (\lambda - \lambda_{ref})$, where we choose $\lambda_{ref} := 2\,\mu$m as arbitrary reference wavelength.

Free parameters of the circumprimary disk are the P.A. (ϕ), angular extent along the major axis (Gaussian FWHM θ_A), and inclination angle (i, measured from the polar axis). Due to temperature gradients in the circumstellar material, it is possible that the source brightness distribution might change with wavelength. To test this hypothesis, we performed our geometric fits both to the complete data set and to the aforementioned data subsets (H, K_1, K_2 wavelength bins).

In order to find the best fit, we employ a Levenberg–Marquardt least-square-fitting procedure and minimize the likelihood estimator $\chi^2_r = \chi^2_{r,V} + \chi^2_{r,\Phi}$, where $\chi^2_{r,V}$ and $\chi^2_{r,\Phi}$ are the reduced least squares between the measured and model visibilities and CPs, respectively (Equations (1) and (2) in Kraus et al. 2009a). For our best-fit solution (Table 2), the uncertainties on the individual parameters have been estimated using the bootstrapping technique. The fit provides a slightly better representation of the CP than the visibility data, as indicated by the $\chi^2_{r,V}$ and $\chi^2_{r,\Phi}$ values. This likely indicates that the circumprimary disk geometry is not well represented by a Gaussian-brightness distribution and we will consider more physical models in an upcoming study (S. Kraus et al. 2012, in preparation).

Given that the position of the companion might change notably between 2008 and 2009, we first fitted only the 2008 data in order to characterize the properties of the stellar components and the circumstellar material.

3.3. Orbital Motion Measurement

Following the detailed characterization of the V921 Sco system for epoch 2008 (Section 3.2), we then investigated whether we find evidence for orbital motion between 2008 and 2009. Compared to 2008, a significantly smaller number of AMBER observations was recorded in 2009 (Table 1), which leads us to fix the geometry of the circumprimary disk using the best-fit parameters from epoch 2008 and treat only the two astrometric parameters (Θ, ρ) and the flux ratio (F_B/F_{tot}) as free fitting parameters.

The resulting best-fit parameters can be found in Table 2 and indicate that the position of the secondary has moved significantly in P.A. ($\sim 7^\circ$) during the covered $\sim$8 months, while only marginal changes in separation ($\rho \lesssim 0.5$ mas) or in the flux ratio could be detected over this time period.

4. INTERPRETATION

4.1. Characterization of the Detected Companion Star

Assuming a face-on circular orbit, we can estimate from the detected signs of orbital motion (Table 2) the period of the orbit to $P \sim 35$ yr. Of course, for a precise mass determination, long-term follow-up observations will be necessary in order to derive the full dynamical orbit.

Table 2
Model-fitting Results for the VLTI/AMBER Continuum Observations (Section 3.2)

Epoch	Spectral	Secondary Star					Circumprimary Disk					
	Band	Θ (deg)	ρ (mas)	θ_B (mas)	$\frac{F_B}{F_{tot}}$ (at 2 μm)	s (μm^{-1})	θ_A (mas)	i (deg)	ϕ (deg)	$\chi^2_{r,V}$	$\chi^2_{r,\Phi}$	χ^2_r
2008	H	353.0	25.0	$\leqslant$0.5	0.074	0[a]	6.12	51.1	143.2	2.46	1.40	1.73
2008	K_1	353.4	25.0	$\leqslant$0.5	0.070	0[a]	6.85	48.6	143.5	2.50	2.14	2.25
2008	K_2	353.1	25.0	$\leqslant$0.5	0.064	0[a]	7.55	48.5	149.0	3.91	1.97	3.27
2008	All	353.8	25.0	$\leqslant$0.2	0.054	−0.0056	7.5	50.3	147.8	4.30	3.09	4.88
		±1.6	±0.8		±0.018	±0.019	±0.2	±1.9	±4.3			
2009	All	347.3	25.5	$\leqslant$0.2[a]	0.054[a]	−0.0056[a]	7.5[a]	50.3[a]	147.8[a]	4.17	1.78	3.39
		±1.0	±1.2									

Note. [a] In our fitting procedure, this parameter was kept fixed.

Both in our images and our model fits, the companion appears spatially unresolved (Gaussian FWHM <0.3 mas, corresponding to <0.35 AU at 1.15 kpc), which suggests that V921 Sco B is not associated with circumstellar material. Based on this result, we can compute the flux ratio of V921 Sco A and B for the H band ($(F_B/F_A)_H = 0.83 \pm 0.15$) and K band ($(F_B/F_A)_K = 1.18 \pm 0.12$). These values suggest that V921 Sco B is of cooler temperature and later spectral type than the primary V921 Sco A, although the current uncertainties are still too large for a quantitative spectral classification.

4.2. Relation with Large-scale Structures

Our IMACS narrowband and broadband images (Figure 1) reveal a remarkably complex environment around V921 Sco. The overall shape of the nebula is bipolar, where the southwestern part appears much fainter and less extended, perhaps indicating that this part is facing away from the observer and therefore suffers from a larger amount of obscuration from material in the ambient cloud. Obscuration from foreground material might also be responsible for the dark filaments that appear in the southeastern part of the nebula (shaded area in Figure 1(G)).

Remarkably, the symmetry axis of the bipolar nebula (50° ± 5°) appears well aligned with the polar axis (57.°8 ± 4.°3) of the AU-scale disk detected with interferometry, suggesting that the nebula might have been shaped through outflow-activity from V921 Sco. From our kinematical modeling (S. Kraus et al. 2012, in preparation), we conclude that the disk is notably inclined, with the northeastern disk axis facing toward Earth. Therefore, based on the measured disk inclination and orientation, one would expect the northeastern lobe of the bipolar nebula to appear brighter, as is observed. This scenario provides a natural explanation for the large number of arc- and cone-shaped structures which can be seen in our IMACS images (Figure 1) and that appear centered on V921 Sco. We have identified the most significant of these arc- and cone-shaped features in our deepest image (R band, Figures 1(E) and (F)). After confirming the features in images taken with other filters, we marked them in Figure 1(G).

The distribution of the individual arc fragments, in particular in the northeastern lobe, suggests that we might observe up to five layers of ejecta, which have been created during episodic events of extreme mass loss. In order to obtain a rough estimate for the period of the mass-loss events, we measured the typical separation between the different layers (4″–5″) and apply a projection factor in order to correct for the system inclination angle of 50.°3 ± 1.°9 (Section 2). Assuming the maximum expansion velocity of 1400 km s^{-1} measured by Borges Fernandes et al. (2009) and a distance of 1.15 kpc, we find that a mass-loss period of ∼25 yr would be required, which seems consistent with the period of the companion, as estimated for a circular orbit (Section 4.1). Compared to the bow-shock structures observed around other high-mass young stellar objects (YSOs; e.g., Kraus et al. 2010b), the arcs around V921 Sco have a clumpy and sometimes truncated structure, possibly indicating a lower degree of collimation in the V921 Sco outflow.

In a field of about 1 arcmin, we detect in our IMACS and FIRE images at least 26 stellar sources. Habart et al. (2003) obtained spectra for a subset of these sources (see identification in Figure 1(I)) and classified them as embedded low- and intermediate-mass YSOs. Increasing the number density in the cluster, our observations strengthen the argument that V921 Sco is likely in a young evolutionary stage and, like many massive YSOs, embedded in a star-forming region of low- and intermediate-mass YSOs.

4.3. Binary Interaction and the B[e] Phenomenon

Our detection of a companion around V921 Sco is interesting in the context of earlier suggestions that the B[e] phenomenon might be related to dynamical interaction in a close binary system, either as a result of a recent stellar merger (e.g., Podsiadlowski et al. 2006) or through material which might have been ejected during phases of binary interaction (e.g., Sheikina et al. 2000; Miroshnichenko 2007; Kraus et al. 2010a). Unfortunately, only very few B[e] stars have been studied so far with sufficient angular resolution to make definite statements about multiplicity. One of the best-studied B[e] systems is HD 87643, where Millour et al. (2009) detected a close companion around this supergiant star. Both the projected separation (∼50 AU) and orbital period (∼50 yr) of this system show similarities with the characteristics we deduce for V921 Sco (∼29 AU, $P \sim 35$ yr). Also, both systems are embedded in an extended nebulosity with a shell-like substructure, indicating episodic mass loss. Therefore, it is plausible that the mass loss in both systems might be triggered by dynamical interaction of the companions with the circumprimary disks. The B[e]-star-characteristic permitted and forbidden line emission might then originate in low-density material which is periodically stripped away from the circumprimary disk. This scenario works independently of the evolutionary status and physics of the circumprimary disks (accretion or excretion disks) and might explain the diversity of stellar systems (Herbig B[e], supergiant, symbiotic star, compact planetary nebulae) in which the B[e] phenomenon is observed.

Follow-up interferometric studies on V921 Sco and HD 87643 might confirm this scenario, for instance by measuring the orbital eccentricity and by imaging the expected star–disk interaction effects during periastron passage.

5. CONCLUSIONS

We have investigated the milliarcsecond-scale environment around the B[e] star V921 Sco and summarize our findings as follows.

1. In our model-independent interferometric imaging, we discover a close (∼25.0 mas) companion and detect signs of orbital motion ($\Delta\Theta \sim 7^\circ$) between the 2008 and 2009 observations. The newly discovered companion V921 Sco B is apparently not associated with a circumstellar disk and likely of later spectral type than the primary, as indicated by the measured $H - K$ color.
2. Around the primary star, our images show a spatially extended disk-like structure, seen under an intermediate inclination angle of $50\overset{\circ}{.}3 \pm 1\overset{\circ}{.}9$.
3. As about half of all B[e] stars (Marston & McCollum 2008), V921 Sco is associated with an extended nebula. In the case of V921 Sco, the nebula has an intriguing bipolar morphology, where the symmetry axis ($50^\circ \pm 5^\circ$) coincides with the polar axis of the AU-scale disk resolved by our interferometric observations ($57\overset{\circ}{.}8 \pm 4\overset{\circ}{.}3$). In our narrowband- and broadband-filter images (Figure 1), we detect complex, partially arc-shaped substructures, which might have been shaped by episodic mass-loss events, possibly triggered by the periastron passage of the newly discovered close companion.
4. Our findings add new support to the hypothesis that the B[e] phenomenon might be a consequence of interaction effects in close multiple systems, where the forbidden line-emitting material is ejected during close companion encounters and then episodically repeated during the periastron passage.

We thank Wen-Hsin Hsu for sharing some Magellan/IMACS observing time. This work was done under contract with the California Institute of Technology (Caltech), funded by NASA through the Sagan Fellowship Program (S.K. is a Sagan Fellow).

Facilities: VLTI, Magellan:Baade, Magellan:Clay

REFERENCES

Acke, B., & van den Ancker, M. E. 2006, A&A, 457, 171
Acke, B., van den Ancker, M. E., & Dullemond, C. P. 2005, A&A, 436, 209
Allen, D. A., & Swings, J. P. 1976, A&A, 47, 293
Benedettini, M., Nisini, B., Giannini, T., et al. 1998, A&A, 339, 159
Boersma, C., Peeters, E., Martín-Hernández, N. L., et al. 2009, A&A, 502, 175
Borges Fernandes, M., Kraus, M., Chesneau, O., et al. 2009, A&A, 508, 309
Borges Fernandes, M., Kraus, M., Lorenz Martins, S., & de Araújo, F. X. 2007, MNRAS, 377, 1343
Chelli, A., Utrera, O. H., & Duvert, G. 2009, A&A, 502, 705
Habart, E., Testi, L., Natta, A., & Vanzi, L. 2003, A&A, 400, 575
Hofmann, K.-H., & Weigelt, G. 1993, A&A, 278, 328
Hutsemekers, D., & van Drom, E. 1990, A&A, 238, 134
Kraus, S., Balega, Y. Y., Berger, J.-P., et al. 2007, A&A, 466, 649
Kraus, M., Borges Fernandes, M., & Chesneau, O. 2010a, in ASP Conf. Ser. 435, Binaries—Key to Comprehension of the Universe, ed. A. Prša & M. Zejda (San Francisco, CA: ASP), 395
Kraus, S., Hofmann, K.-H., Benisty, M., et al. 2008, A&A, 489, 1157
Kraus, S., Hofmann, K.-H., Malbet, F., et al. 2009a, A&A, 508, 787
Kraus, S., Hofmann, K.-H., Menten, K. M., et al. 2010b, Nature, 466, 339
Kraus, S., Weigelt, G., Balega, Y. Y., et al. 2009b, A&A, 497, 195
Kreplin, A., Kraus, S., Hofmann, K.-H., et al. 2012, A&A, 537, A103
Kurucz, R. L. 1970, SAO Special Report, 309
Lamers, H. J. G. L. M., Zickgraf, F., de Winter, D., Houziaux, L., & Zorec, J. 1998, A&A, 340, 117
Marston, A. P., & McCollum, B. 2008, A&A, 477, 193
Mérand, A., Bordé, P., & Coudé Du Foresto, V. 2006, A&A, 447, 783
Millour, F., Chesneau, O., Borges Fernandes, M., et al. 2009, A&A, 507, 317
Miroshnichenko, A. S. 2007, ApJ, 667, 497
Oudmaijer, R. D., Baines, D., Porter, J. M., & Pozzo, M. 2006, in ASP Conf. Ser. 355, Stars with the B[e] Phenomenon, ed. M. Kraus & A. S. Miroshnichenko (San Francisco, CA: ASP), 99
Petrov, R. G., Malbet, F., Weigelt, G., et al. 2007, A&A, 464, 1
Podsiadlowski, P., Morris, T. S., & Ivanova, N. 2006, in ASP Conf. Ser. 355, Stars with the B[e] Phenomenon, ed. M. Kraus & A. S. Miroshnichenko (San Francisco, CA: ASP), 259
Richichi, A., Percheron, I., & Khristoforova, M. 2005, A&A, 431, 773
Sheikina, T. A., Miroshnichenko, A. S., & Corporon, P. 2000, in ASP Conf. Ser. 214, IAU Colloq. 175: The Be Phenomenon in Early-Type Stars, ed. M. A. Smith, H. F. Henrichs, & J. Fabregat (San Francisco, CA: ASP), 494
Simcoe, R. A., Burgasser, A. J., Bernstein, R. A., et al. 2008, Proc. SPIE, 7014, 70140U
Tatulli, E., Millour, F., Chelli, A., et al. 2007, A&A, 464, 29